Dynamics of disordered patterns in electroconvection of homeotropically aligned nematic liquid crystals

P. Tóth,[1,2] Á. Buka,[2] J. Peinke,[1] and L. Kramer[1]
[1]*Universität Bayreuth, D-95440 Bayreuth, Germany*
[2]*Research Institute for Solid State Physics, P.O. Box 49, H-1525 Budapest, Hungary*
(Received 30 December 1997; revised manuscript received 6 April 1998)

We report on experiments in nematics with homeotropic alignment where the electrohydrodynamic instability occurs after a bend Freedericksz transition. The threshold of convection, the wave number at onset, and the threshold for the transition between order and disorder in the presence of a stabilizing magnetic field agree with theory. Whereas in the oblique-roll range the behavior of the correlation time of the disordered state exhibits near onset the expected scaling behavior, the disordered state in the normal-roll range at zero magnetic field shows no dynamics below a well-defined value ε_s of the reduced control parameter, in contrast to theoretical predictions. At ε_s one has reproducibly a continuous and reversible transition to a dynamic state. We attribute these features to the appearance of chevronlike structures. [S1063-651X(98)01308-7]

PACS number(s): 61.30.Gd, 47.20.Ky, 47.65.+a

I. INTRODUCTION

ac driven electrohydrodynamic convection (or electroconvection, EC) in nematic liquid crystal layers has been studied experimentally and theoretically for about 30 years [1]. Most of the work involved cells with planar homogeneous alignment where the director $\hat{\mathbf{n}}$ is (ideally) anchored at the bounding plates along a fixed direction (x) parallel to the plates, which define the x-y plane [2–4]. The director $\hat{\mathbf{n}}$ represents the local axis of average molecular orientation in the nematic. For materials with negative or slightly positive dielectric anisotropy ϵ_a and nonvanishing conductivity, which is due to the presence of some ionic impurities, EC sets in in the form of spatially periodic convection rolls at a threshold $V_c(f)$ depending on frequency f. Since the flow is coupled to periodic distortions of the director, the pattern is easily visualized. The patterns at threshold are in most cases stationary. They are characterized by a two-dimensional in-plane wave vector $\vec{k}_c=(q_c,p_c)$, describing the orientation and spacing of the rolls (q_c and p_c are the x and y components of k_c).

The first model of EC, based on the Carr-Helfrich mechanism for charge separation in media with anisotropic conductivity, was given in 1969 [5]. This dc treatment was readily generalized to the ac case [6], where besides the ''conduction mode'' appearing at low frequencies, one also has the ''dielectric mode'' above the crossover frequency f_d. In this early one-dimensional treatment one cannot capture the wave vector of the patterns. The two-dimensional analysis of the nematodynamic equations [7] allows one to describe the most common case where the rolls are oriented perpendicular to the director alignment, i.e., $p_c=0$ (''normal rolls''). At low frequencies one has often rolls that are oriented obliquely, with the roll angle going to zero at the so-called Lifshitz point f_L [8]. To capture these features one has to go to a three-dimensional treatment [9,2,10].

The threshold behavior sketched above is well described by a linear stability analysis (LSA) of the basic (nonconvecting) state starting from the standard hydrodynamic equations. This analysis cannot capture nonlinear properties, such as, e.g., the amplitude of the pattern as a function of the reduced control parameter commonly defined as $\varepsilon=V^2/V_c^2-1$. The next step then is a weakly nonlinear analysis, which employs an expansion in terms of the amplitude including slow modulations in space and time of the patterning mode. At leading nontrivial order one is left with a Ginzburg-Landau equation for the complex amplitude A describing amplitude and phase modulations. This equation describes, among others, the band of wave vectors for which periodic solutions exist above threshold, the (slow) evolution towards the stable part of these states [11,2,10], and the motion of defects [12]. Further above threshold one typically has to resort to numerical Galerkin methods to calculate the periodic roll solutions and their stability [10,13,14], although generalized weakly nonlinear schemes are possible [15].

Efforts to investigate homeotropically oriented cells using nematics with manifestly negative ϵ_a were initiated rather recently; see [16–20] for experimental and [21,10,22] for theoretical work. In this case the director is oriented perpendicular to the layer, i.e., in the z direction so that in the initial state the system is isotropic in the x-y plane. In this case the first instability is the (ideally) spatially homogeneous (in the x-y plane) Freedericksz transition where the director bends away from the z direction, singling out spontaneously a direction $\hat{c}$ in the x-y plane. This corresponds to a spontaneous breaking of an O(2) symmetry. After the transition the slow variation of the in-plane director $\hat{c}$ may be described by an angle φ. Furthermore the isotropy may also be broken externally by applying a (weak) stabilizing magnetic field parallel to the plane (x direction).

At higher voltages there is a further transition to electroconvection, which is in many respects similar to that in cells with planarly aligned nematics. However, the homeotropic case with full rotational invariance (i.e., without additional magnetic field) differs in a fundamental way from the planar case, since the spontaneous breaking of the continuous O(2) symmetry leads in the Freedericksz distorted state to a Goldstone mode, i.e., an undamped mode of the system describ-

ing the (infinitesimal) rotation of the in-plane director. This mode has to be incorporated into the weakly nonlinear description of the system, since the patterning mode will have an effect on the Goldstone mode at arbitrarily small amplitude, i.e., the convection rolls will in general exert a torque on the in-plane director. The in-plane director, on the other hand, acts back on the patterning mode. As was suspected for some time [21] and shown recently [22], this coupling leads to destabilization of all roll solutions and apparently to spatiotemporal chaos at the threshold of convection. In fact, disordered states have been observed experimentally [16–20]. In spite of the disorder one can distinguish also in the homeotropic case between a variety of patterns in particular (disordered) normal and oblique rolls. From simulations of the generalized weakly nonlinear equations the correlation time in the disordered state was determined at selected frequencies [22]. Some measurements of this quantity have already been presented [19,20].

A stabilizing magnetic field suppresses the disorder up to some value ε_u [18–20], which can be calculated either by a numerical Galerkin procedure [23] or, near threshold, by the generalized weakly nonlinear analysis [22]. As became clear recently, the destabilization of normal rolls occurs either through a long-wavelength undulatory (zigzag) instability (f not too far above f_L) leading to a disordered state, or, at higher frequency, through a homogeneous instability leading to ''abnormal rolls'' where the in-plane director is rotated homogeneously in the x-y plane out of its normal orientation [22,24] (see also [14] for the analogous scenario in the planar case). Actually, normal rolls at zero magnetic field, i.e., in the disordered state, also exhibit the symmetry breaking typical for abnormal rolls, and in fact they were first discovered experimentally in this context [17].

We point out that under certain conditions (predominantly near the crossover frequency f_d for materials with negative dielectric anisotropy) one may have traveling rolls in the conduction regime, which arise via a Hopf bifurcation. To describe this feature one has to generalize the standard hydrodynamic description of nematics, where the material is treated as an anisotropic Ohmic conductor, in favor of a description in terms of a weak electrolyte [26]. The weak electrolyte effects also have the consequence that in some range below the crossover point from stationary to traveling rolls one typically has a slightly subcritical bifurcation with a small hysteresis [27]. The theory has been developed only for planar alignment, but one expects similar behavior in the homeotropic case. Although in our cells we could observe traveling waves near f_d, in the results presented here we are well below the crossover, so weak electrolyte effects are presumably not relevant here.

In this paper we present experimental results for cells with homeotropic alignment. The experimental setup and some details of the measurement procedures are described in Sec. II. The results are presented in Sec. III. First, in Sec. III A, the Freedericksz transition and the ensuing Freedericksz distorted state are discussed. Although some of the linear properties of the transition to EC and the various evolving patterns have been studied before, we first present in Sec. III B these results in order to compare them with theory. In Sec. IV A the transition between order and disorder in the presence of a magnetic field is characterized. A novel structure, chevrons, is found in the conduction regime, which in fact has been predicted from the generalized weakly nonlinear theory [25] and which are presented briefly in Sec. IV B. In Sec. IV C we present our results on the dynamics of the disordered states in the absence of a magnetic field, as extracted from the temporal correlation of the optical contrast. Of particular interest are the frozen states obtained in the normal-roll range for ε below a value ε_s, which decreases with increasing frequency. The frozen states are characterized by having (locally) a chevron structure. The transition to a dynamical state at ε_s has the properties of a continuous (reversible) bifurcation. Finally, in Sec. V we discuss the novel features found.

II. EXPERIMENTAL SETUP

The usual capacitor-type cell was used where the nematic layer (in the x-y plane) is sandwiched between two glass plates coated with a transparent electrode (ITO). The plates were separated by thin Mylar spacers of nominal thickness d about 30 μm. The lateral sizes of the cells were of order 1 cm$\times$1 cm. In order to achieve homeotropic anchoring of the director the inner surfaces of the plates were treated either with the surfactant DMOAP (dimethyloctadecyl[3-(trimethoxysilyl)-propyl]ammonium chloride) or alternatively with lecithine. The cell was filled with the standard nematic material MBBA [N-(4-methoxybenzylidene)-4-butylaniline]. An ac voltage was applied across the layer by a PC-driven function generator. The rms amplitude V and frequency f of the applied voltage are the usual control parameters, but in some experiments we have also applied a magnetic field $\vec{H}\|\hat{x}$. The maximum value of the magnetic induction $B=\mu_0 H$ reached by the conventional electromagnet was 0.32 T. The temperature was stabilized at 25.0 $\pm$0.1 °C by a thermostatted water cycle.

An area of the cell up to 1 mm^2 was observed either with a long-range microscope from a distance of about 30 cm or with a traditional microscope, depending on whether the electromagnet was used or not. In both cases magnifications up to 100$\times$ were used. A charge-coupled device (CCD) camera was mounted onto both microscopes and connected to a frame grabber card that digitized the images with a spatial resolution of 512$\times$512 pixels and 256 gray scales. Whereas the Freedericksz distorted state was monitored under crossed polarizers, convection was observed by the shadowgraph method with only one polarizer [28]. Here maximum contrast is expected when the light is polarized along the in-plane director.

Although the cells used in the experiments have been sealed in order to avoid aging effects in the liquid crystal material, their conductivity remained fairly constant only for about one month before increasing more rapidly. During the first month, when experiments were done, the crossover frequency increased by less than 10%. Experimental runs did not exceed 3 days. Changes of f_d during this period were undetectable. To perform all experiments several cells were necessary. In Table I the various cells are listed together with the relevant EC threshold data. The cells, which have been used to obtain the results shown in the figures, are indicated in the captions.

TABLE I. Parameters of the cells used; notations: *hl*: orientation with lecithine, *ho*: orientation with DMOAP, ⋆: thickness d measured by IR spectrometry (otherwise thickness of spacer).

Cell	d [μm]	f_d^{expt} [Hz]	$V_c(f_d)$ (V)	f_L^{exp} (Hz)	V_c(10 Hz) (V)
*hl*01	47⋆	594	93.20	271	6.13
*hl*04	28	728	67.34		6.01
*hl*05	28	710		240	7.04
*hl*07	33⋆	921		284	
*hl*12	35⋆	845	98.34	290	7.75
*ho*06	25⋆	895	96.10	308	5.84
*ho*07	23	910	94.32	321	5.68
*ho*11	28⋆	940		329	6.05
*ho*13	27⋆			324	6.87
*ho*14	23	933	97.30	330	7.03
*ho*25	23			334	
*ho*27	23			330	6.20
*ho*31	23			332	

III. SUBTHRESHOLD BEHAVIOR AND ONSET OF EC

A. The Freedericksz distorted state

Given the negative dielectric anisotropy ϵ_a and the positive diamagnetic anisotropy χ_a of MBBA the homeotropically aligned director field first undergoes a bend Freedericksz transition when the voltage V along z or the magnetic induction B along x exceed their respective threshold values

$$V_F=\pi\left(\frac{k_{33}}{|\epsilon_a|\epsilon_0}\right)^{1/2},\quad B_F=\frac{\pi}{d}\left(\frac{k_{33}}{\chi_a\mu_0^{-1}}\right)^{1/2}. \tag{1}$$

Here k_{33} is the elastic constant for bend deformation.

We first determined V_F and B_F. The intensity I of light passing through the cell between crossed polarizers was recorded while either V or B (one being zero) was increased in steps of 0.05 V or 0.005 T every 2 min. The threshold was determined by a linear regression of the I versus V or B curve to its value I_0 in the initial state. The values $V_F=3.74\pm0.15$ V and $B_F=0.263\pm0.01$ T measured in this way agree within the experimental uncertainty with the ones calculated from Eq. (1) using the material parameters of MBBA I in [2] and $\chi_a=0.97\times4\pi\times10^{-7}$. Because of this agreement between experiment and theory as well as because of the abrupt increase of I at V_F or B_F we can exclude pretilt and weak anchoring of the director in the cells used in the experiments.

When the electric and magnetic fields are applied simultaneously the values $V_f(B)$ and $B_f(V)$ at threshold are related by

$$\left(\frac{V_f}{V_F}\right)^2+\left(\frac{B_f}{B_F}\right)^2=1. \tag{2}$$

This relationship is satisfied experimentally with an accuracy of about 4%. We mention that V_f and V_F are—as expected—independent of the frequency of the applied voltage.

One should note that, as pointed out before, the purely electrically driven Freedericksz transition has a different character from that when a magnetic field is present. In the latter case the magnetic field singles out a preferred axis (x) in the plane of the layer along which the director bends. There is a twofold degeneracy of the Freedericksz distorted states with domain walls separating them. For zero magnetic field the director can bend in any direction (complete degeneracy) in the x-y plane and one has point defects (umbilics). A snapshot of a state that appears right after the transition (without magnetic field) containing several umbilics is shown in Fig. 1. These structures disappear on a time scale of about 10 min, after which the director field will be homogeneous over rather large areas.

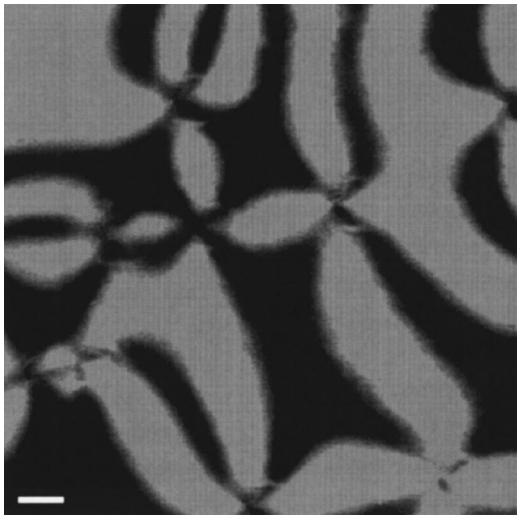

FIG. 1. ''Schlieren'' textures appearing immediately after an electrically driven bend Freedericksz transition between crossed polarizers. The grey scale encodes the orientation of the in-plane director modulo $\pi/2$. The scale bar shows 100 μm (cell *ho*13).

B. Behavior at threshold of EC

In the Freedericksz distorted state ($V>V_F$) at $H=0$ the director was allowed to relax for typically 1 h. Then the voltage was gradually increased in order to determine the threshold $V_c(f)$ for convection, which is now a function of the applied frequency (contrary to V_F). The voltage was increased in intervals of 1 min by steps of 0.05 V. At each step the contrast, i.e., the rms value of the intensity along one line of the picture, was determined, and $V_c(f)$ was extrapolated by a linear fit. The measurement was carried out by increasing and decreasing the voltage. The frequency range was covered from 10 to about 600 Hz by steps of 10 Hz, staying within the conduction range.

The measured threshold voltage versus frequency is shown in Fig. 2 (only every third measurement is plotted). Although the evolving patterns are more or less disordered one can distinguish near onset between normal and oblique rolls; see Fig. 3. Oblique rolls, marked by open circles, and normal rolls, marked by filled circles, occur below and above the Lifshitz frequency f_L respectively (Fig. 2). For frequencies well below f_L one finds both directions of the rolls (zig and zag) superposed as shown in Fig. 3(b). Also shown in Fig. 2 is a prediction of the threshold $V_c(f)$ as obtained from the linear stability analysis of the full equations (LSA) [29] (line). The value of the conductivity of the material was slightly adjusted as usual in order to fix the frequency scale

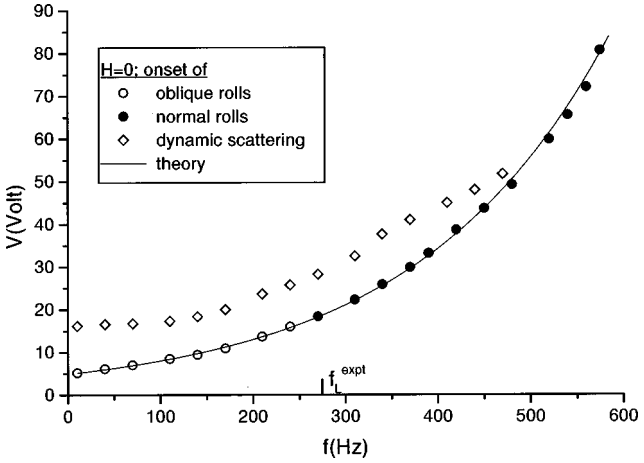

FIG. 2. Voltage vs frequency phase diagram. The symbols indicate the onset of the respective patterns (cell $hl01$). The continuous line is the threshold $V_c(f)$ calculated from the linear stability analysis (LSA).

leading to $\sigma_\perp = 7.8\times10^{-8}(\Omega\ \mathrm{m})^{-1}$. Moreover, in Fig. 2 the measured transition from disordered patterns involving relatively slow dynamics to the more turbulent dynamic scattering state (diamonds) occurring at fairly large ε is included. Although this will not be discussed here, we want to mention, that—as in the planar case—we found at very large ε a transition between the type I and II dynamic scattering modes [1].

In order to determine the wave vector $\vec{k}_c = (q_c, p_c)$, and in particular the tilt angle (obliqueness) of the rolls at onset, a voltage jump from below to just above threshold, $\varepsilon \sim 0.04$, was applied. Shortly afterwards a snapshot of the pattern was taken, because the angle between the rolls changes with time. The wave vector could be determined from a 2D Fourier analysis of the snapshots, in spite of the fact that the rolls can have an arbitrary orientation. The reason is that, as pointed out before, the shadowgraph method, which makes use only of one polarizer, has maximum sensitivity when the light is polarized along the in-plane director $\hat{c}$ (zero intensity in the perpendicular direction). Therefore the Fourier spectrum, which is distributed over a ring of radius $|\vec{k}_c|$, exhibits peaks corresponding to patches where $\hat{c}$ is parallel to the polarizer. Thus, in the normal-roll range one has two peaks at angles 0 and π with respect to the polarizer, and in the oblique-roll range one has four peaks that allow one to extract the angle of oblique rolls. In Fig. 4(a) the results for p_c/q_c are shown

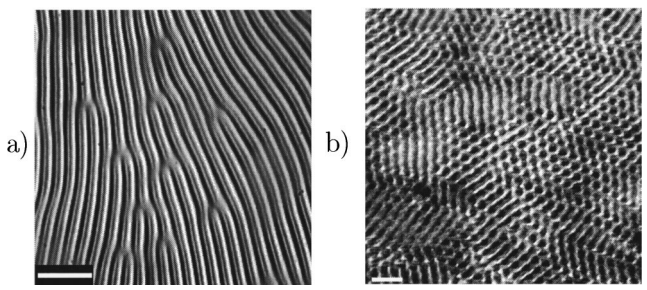

FIG. 3. Snapshots of (a) normal (cell $ho25$ at $f = 1.04 f_L$) and (b) oblique rolls near threshold (cell $hl07$ at $f = 0.1 f_L$). In (b) one sees the superposition of zig and zag. The scale bars are 100 μm.

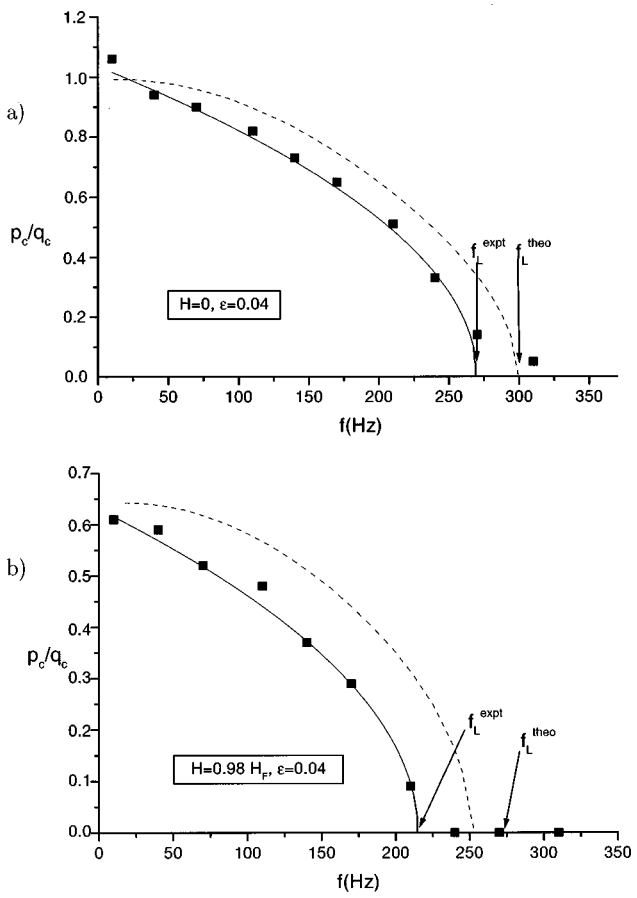

FIG. 4. Obliqueness of the rolls (a) without and (b) with an additional stabilizing magnetic field ($H = 0.98 H_F$) (cell $hl01$). The dashed curves are predictions of the LSA using the same material parameters as in Fig. 2. The continuous curves represent the function $\alpha(f_L - f)^{1/2}$ with fit parameters $\alpha = 0.04$, $f_{L,H=0}$ (cf. Table I), and $f_{L,H=0.98H_F} = 214$ Hz.

as a function of the frequency f. They have been fitted by a square-root law $\alpha(f_L^{\mathrm{expt}} - f)^{1/2}$ (continuous line), which is expected to hold near f_L. Also shown is the theoretical prediction as obtained from the LSA [29] (dotted line) using the same parameters as before. Note that the agreement is better than in previous work [18]. The remaining discrepancy between the theoretical and the measured values of f_L is likely to be the result of uncertainties in the material parameters. Some later measurements are related to f_L^{expt} (Sec. IV C). Then a more precise determination of f_L^{expt} was done by choosing smaller frequency steps in the vicinity of f_L^{expt}. We estimate the error to be below about ± 4 Hz.

Similar measurements were performed in the presence of a stabilizing magnetic field $\vec{H} \| \hat{x}$. Besides producing well-ordered patterns [18] (see also next subsection) H shifts V_c upward and changes also the critical wave vector. In particular the Lifshitz point is shifted to lower frequency and the wave number is increased (wavelength decreased). The results for p_c/q_c as well as the predictions of LSA are shown in Fig. 4(b). In Fig. 5 we present a comparison between experiment and theory of the wavelength $\lambda = 2\pi/k_c$ of the pattern. Similar measurements in planarly aligned cells also show a square-root behavior of the roll angle versus fre-

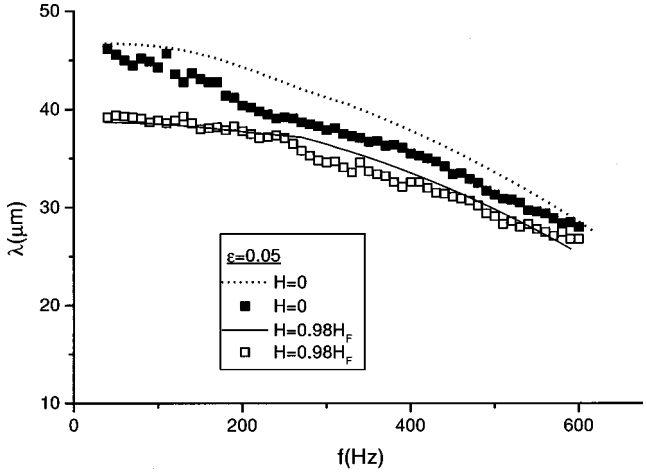

FIG. 5. Wavelength of the pattern vs frequency without and with magnetic field. The curves represent the results from LSA (cell *hl*01).

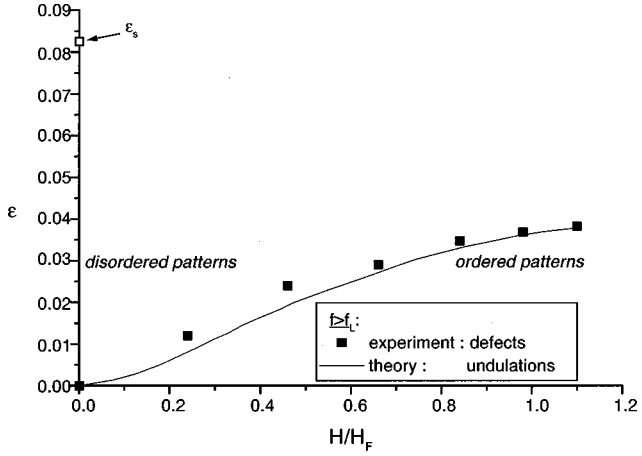

FIG. 7. Onset ε_u of instability of rolls vs reduced magnetic field. At zero field the value for ε_s, where dynamic sets in, has been included (open square) (cell *hl*07).

quency; see [30] for results on the material I52, and [31] for the material Merck Phase 5.

The measurements presented in Figs. 4 and 5 are restricted to a frequency range well below the crossover point to traveling waves. Here one expects, as pointed out before, the bifurcation to be supercritical [27], so that finite amplitude effects presumably are of minor importance.

IV. STATIC AND DYNAMIC CONVECTION STATES

A. Transition to static disorder in the presence of a magnetic field

By applying a magnetic field in the plane of the layer ($\vec{H}\|\hat{x}$) a stabilizing torque is exerted on the director. Then, at the threshold of convection, the situation becomes similar to that in planarly aligned cells, so that the oblique or normal rolls become well-ordered over the whole cell [18]. Now the transition to disorder occurs at a value $\varepsilon_u > 0$ depending on the magnetic field strength [23,22]. We find that the destabilization of the normal rolls occurs in most cases via creation of dislocations in the patterns. Undulations with long wavelength (zigzag instability) as shown in Fig. 6, which are predicted by theory to be the first destabilization of the ordered normal rolls, due to their long wavelength are not always detectable. This explains the discrepancy in Fig. 7 between the measured values of ε_u (appearance of defects) for different field strengths and the theory (appearance of undulations) [29]. Moreover the values at low field are not very accurate. The theoretical curve has been obtained from full numerical calculations without adjustable parameters. From the analytic work a parabolic behavior $\varepsilon_u \propto (H/H_F)^2$ is expected for low fields [22]. The disordered state attained beyond the instability appears to be static in the normal-roll range. This frozen state and the transition to dynamics has been studied in detail only at zero magnetic field and will be discussed below.

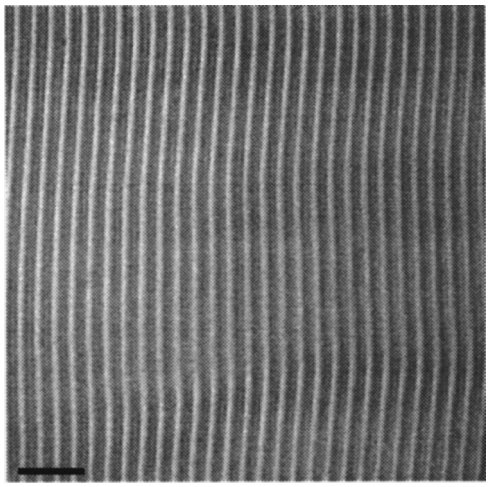

FIG. 6. Initial stage of the undulatory instability in the presence of a magnetic field. $H = 0.3H_F$, $\varepsilon = 0.1$, $f = 1.13 f_L$. The scale bar shows 100 μm (cell *hl*07).

B. Patterns above threshold without magnetic field

In Fig. 8(b) a typical pattern in the normal-roll range is shown. One has defects (dislocations in the roll patterns) ordering along chains, which in the absence of a preferred direction are bent on a long scale. The polarity of defects alternates from chain to chain. A remarkable similarity between the patterns observed here and the chevron patterns known from the dielectric range—especially those observed in thick ($d \sim 100\ \mu$m) planar cells—should be mentioned;

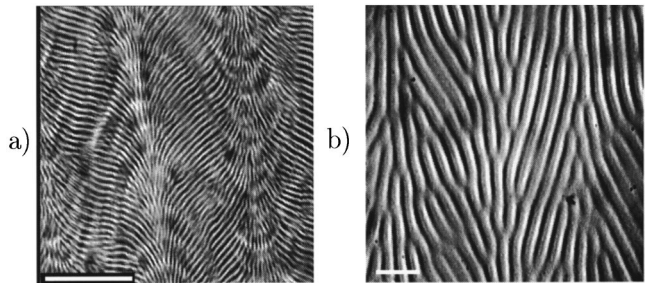

FIG. 8. Chevrons in the dielectric range of electroconvection in a planar nematic (a) and similar pattern (with very different wavelength) in the conduction range ($f > f_L$) of EC in homeotropically aligned nematics (b) (cell *ho*31). In (b) the camera was turned in order to give a better impression of chevrons. In both pictures the bars have the length of 100 μm.

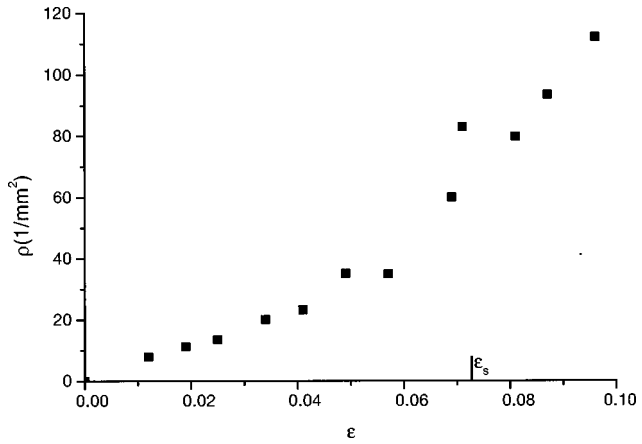

FIG. 9. Density ρ of defects (average over 10 measurements) in the homeotropic chevron state at $f=1.12\,f_L$ (cell *ho*14).

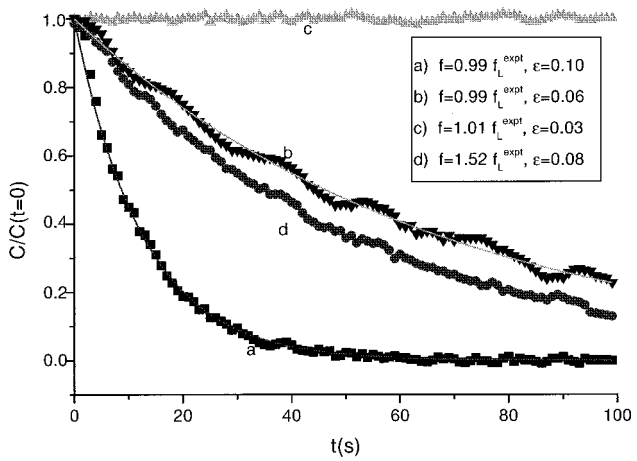

FIG. 10. Temporal behavior of the correlation function for several frequencies in the vicinity of the Lifshitz point (cell *ho*06). The curves *a*, *b*, and *d* have been fitted by exponentials $\exp(-t/\tau_c)$.

see Fig. 8(a). In fact, on the theoretical side a connection between the two systems can be made [25]. In Fig. 9 we show the density ρ of defects in the homeotropic chevron state as a function of ε. At about $\varepsilon=0.07$ the state becomes dynamic (see below).

C. Transition from static to dynamic disorder without magnetic field

Next, the time evolution of the patterns was studied as a function of ε and f. After the desired values of ε and f were applied the pattern was allowed to relax over a period of typically 5 min. Then the contrast K along a line was measured in intervals of 3 s. For small ε the temporal behavior of K was significantly different in the normal and the oblique-roll regime. Whereas in the oblique-roll range the contrast changed rapidly on a scale of the order of 10 s, in the normal-roll range for ε below some critical value ε_s ($\varepsilon_s \sim 0.08$ for f slightly above f_L) no changes could be detected over times longer than 1 h. This shows that beyond f_L the orientation of the director in the x-y plane does not change, because the contrast K depends on the angle between the director and the polarizing direction of the incoming light.

To characterize the dynamics of the director quantitatively the autocorrelation function $C(t)=\langle I(\vec{r},t+t_0)I(\vec{r},t_0)\rangle-\langle I(\vec{r},t_0)\rangle\langle I(\vec{r},t_0)\rangle$ of the intensity I was measured, see Fig. 10 ($\langle\cdots\rangle$ denotes an average over time t_0 and camera line $\vec{r}$). The correlation time τ_c was determined by fitting $C(t)$ to $C_0\exp(-t/\tau_c)$. For $f<f_L^{\mathrm{expt}}$ (oblique rolls) the correlation function decays for any $\varepsilon>0$. The correlation time decreases with increasing ε and increases—at least near f_L—with increasing f. In agreement with the theory [22], which predicts spatiotemporal chaos at the onset, we find in good approximation that $\tau_c^{-1}\propto\varepsilon$. Figure 11(a) shows straight-line fits to these measurements and in Fig. 11(b) the slopes a determined in this way are presented as a function of the reduced frequency.

As pointed out before, in the normal-roll range ($f>f_L$) the pattern is frozen at onset and remains stationary in the range $\varepsilon<\varepsilon_s$ (see curve *c* of Fig. 10). Above ε_s the patterns become dynamic and the correlation function decays in a similar way as in the oblique-roll range (see curve *d* in Fig. 10). Similar measurements, but mainly in the normal-roll range, are shown in Fig. 12 (a different cell was used here). τ_c appears to diverge when approaching ε_s from above. Above ε_s one can fit τ_c^{-1} versus ε by a straight line. In the normal roll range the slope a depends very little on the frequency f. At ε_s one seems to have a sharp and reversible

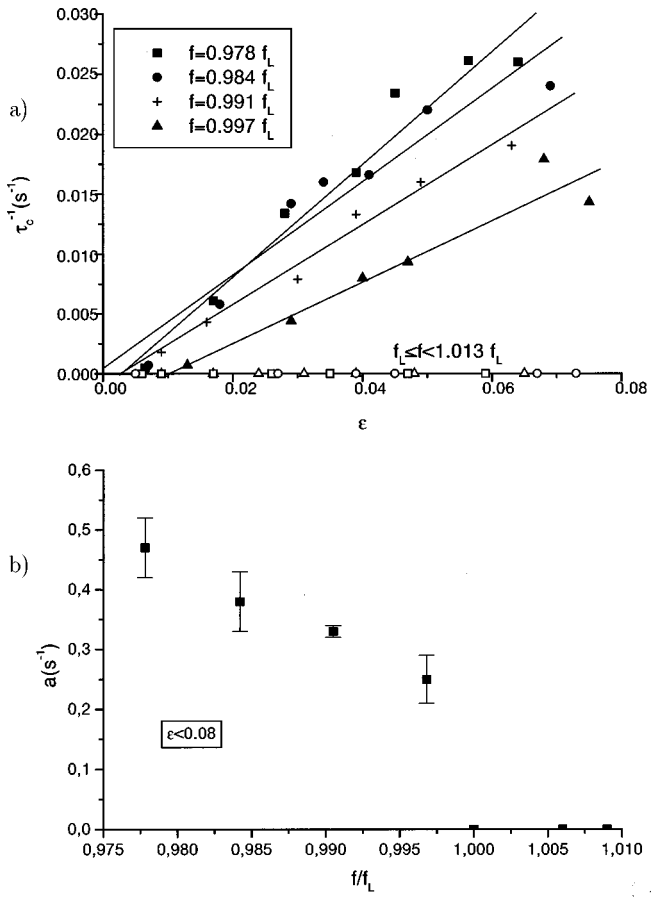

FIG. 11. (a) Inverse correlation time τ_c^{-1} vs ε below and very slightly above the measured Lifshitz point with straight-line fits. The slopes a are given in (b). Note the abrupt drop of a to 0 at the Lifshitz point [(a) and (b): cell *ho*14].

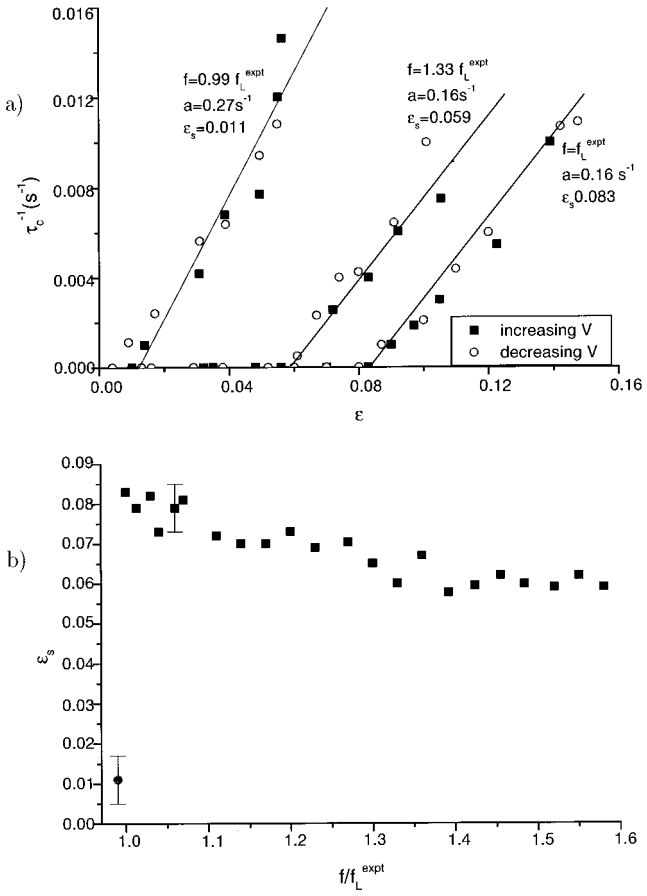

FIG. 12. (a) Inverse correlation time τ_c^{-1} vs ε very slightly below, at, and well above the measured Lifshitz point with straight-line fits. The frequency dependence of ε_s is shown in (b) [(a) and (b): cell $ho27$].

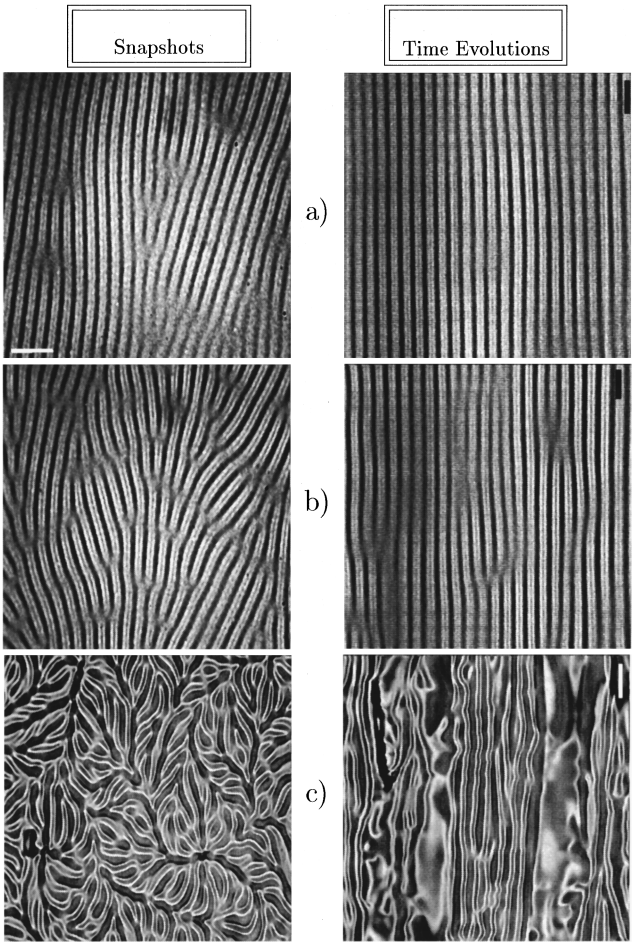

FIG. 13. Snapshots (left row) and x-t plots (right row) of typical patterns in the normal-roll range ($f=1.13f_L$) in the static and dynamic regime (cell $ho07$). From top to bottom: (a) $\varepsilon=0.06$; (b) $\varepsilon=0.09$; (c) $\varepsilon=0.21$. The horizontal scale bar in (a) gives the scale of 100 μm, the vertical bars denote: 200 s in (a) and 1 s in (b) and (c).

crossover between the stationary and dynamic behavior. Thus our results indicate a forward bifurcation. So the situation in the normal roll range seems to be quite different from that in the oblique roll range: for $f<f_L$ we find (at least near f_L) a sensitive dependence of $d\tau_c^{-1}/d\varepsilon$ on f and $\varepsilon_s \approx 0$, whereas for $f>f_L$ $d\tau_c^{-1}/d\varepsilon$ does not seem to depend on f, but there is a manifestly nonzero ε_s, which decreases slightly with increasing f as Fig. 12(b) shows. From the experiments we cannot claim that this change of behavior occurs abruptly, but the crossover has to take place within an interval of about 2 Hz. The behavior in the normal roll range does not yet have a theoretical explanation, but it could be connected with the chevrons appearing in the frozen states (see Sec. V).

Figure 13 shows the patterns observed in the normal-roll range for three values of ε in the static and dynamic regime. On the left side we show snapshots whereas on the right side x-t plots of a line are exhibited. Clearly, at $\varepsilon=0.09$, one still has chevron like ordering.

Similar measurements of the correlation time were presented at two frequencies well below and above the Lifshitz point by Kai and collaborators [19,20]. They used a cell of thickness 50 μm filled with MBBA that was doped with TBAB to obtain a rather large conductivity of $\sigma_\perp = 2.3\,10^{-7}(\Omega\ \mathrm{m})^{-1}$ and a crossover frequency f_d of about 2.6 kHz. In the range where we have static disorder they actually find slow dynamics $\tau_c^{-1} \approx 0.15\varepsilon\ \mathrm{s}^{-1}$. However, at $\varepsilon \approx 0.08$, they find a marked change in slope to about $\tau_c^{-1} = 0.7\varepsilon\ \mathrm{s}^{-1}$. In our measurements we can rule out a slow dynamics below ε_s as found by the authors of Refs. [19, 20]. We attribute this discrepancy to the difference in the cell and material characteristics.

V. CONCLUDING REMARKS

Our measurements have uncovered a number of new features in EC of a homeotropically aligned nematic with negative dielectric anisotropy. The fact that in the absence of a magnetic field complex patterns appear directly at threshold can be considered as established. The surprising feature found here is that in the normal-roll range the state at threshold is static, whereas theory predicts a dynamic situation [22,24]. We do not believe that our results are related to imperfections (inhomogeneities) of our cells leading to pinning effects. The experiments have been repeated with several cells that were manufactured using different materials and methods for the orientation of the nematic (see Sec. II). The results of the different experiments are consistent with each other. The values for ε_s do not differ by more than

about 20%. Another indication that the behavior found is really intrinsic, is, in our view, the observed reversible, bifurcation-type transition between the static and the dynamic state when ε crosses ε_s (see Fig. 12). Due to the uncertainty in the determination of f_L of about ± 4 Hz we cannot really claim that the crossover from the dynamic to the static behavior occurs precisely at the Lifshitz point, but there remains the fact that the qualitative behavior changes within a frequency interval of about 2Hz.

Consequently one concludes that below ε_s an intrinsically stable, static state is established. It appears plausible that this state is associated with the observed chevron-type ordering, which represents a novel feature in this system. As a next step, which goes beyond the scope of the present work, this structure has to be characterized quantitatively as a function of ε and f. At present we may say that the density of defects increases and the average spacing of the defect chains decreases when ε and f are increased. Slightly above ε_s there remains a chevron-type structure. Thus one presumably has a transition between static and dynamic versions of chevrons. A weak magnetic field leads to a long-range ordering of the chevron chains, which otherwise are curved on a slow scale. For stronger fields the chevrons are destroyed. This latter transition is the one discussed very briefly in Sec. IV A. It should be investigated in more detail in future work.

From the work of Kai *et al.* [20] one may conclude that under different conditions (thicker cells, higher conductivity) the state below ε_s is not fully static. However, there remains a transition from slow to faster dynamics, which presumably has the same origin as our observation and is of similar interest.

For the theoretical side one must conclude from our work (at least tentatively) that the generalized weakly nonlinear theory for EC in homeotropic cells as it stands [22,24] is, in spite of its successes, in particular in providing a first mechanism for the formation of chevrons [25], not quite complete. Simulations with this theory have not yielded a static state in the absence of a stabilizing magnetic field. In fact, there the chevrons retain a chaotic dynamics, as is observed in the conventional chevrons in the dielectric range [32]. Possibly the vicinity of the Lifshitz point, where the coherence length in the y direction goes to zero, has to be taken into account. An investigation of this effect is under way. Also, we would not completely rule out the possibility that nonadiabatic effects, which couple the fast scale of the roll pattern with the slow modulations are responsible for the stabilization of chevron-like structures. Clearly EC in homeotropically oriented nematics is an interesting system deserving further study.

Finally it might be worth pointing out that the complex Ginzburg-Landau equation for anisotropic systems yields ordered chevron-like structures that can be static or dynamic [33].

ACKNOWLEDGMENTS

We have benefitted from discussions with W. Pesch, A. G. Rossberg, N. Éber, and C. Haite. Financial support by the TMR program of the EU (network ''Patterns, Noise, and Chaos,'' ERB FMRX-CT 96-0085), the Volkswagen foundation, the Deutsche Forschungsgemeinschaft (KR 690/12), and MTA OTKA T014957 is gratefully acknowledged.

[1] S. Chandrasekhar, *Liquid Crystals* (Cambridge University Press, Cambridge, 1992); P. G. de Gennes and J. Prost, *The Physics of Liquid Crystals* (Clarendon Press, Oxford, 1993); L. M. Blinov, *Electrooptical and Magnetooptical Properties of Liquid Crystals* (John Wiley, New York, 1983).

[2] E. Bodenschatz, W. Zimmermann, and L. Kramer, J. Phys. (France) **49**, 1875 (1988).

[3] I. Rehberg, S. Rasenat, and V. Steinberg, Phys. Rev. Lett. **62**, 756 (1989).

[4] Sh. Kai, N. Chizumi, and M. Kohno, Phys. Rev. A **40**, 6554 (1989).

[5] W. Helfrich, J. Chem. Phys. **51**, 4092 (1969).

[6] Orsay Liquid Crystal Group, Phys. Rev. Lett. **26**, 1642 (1970); E. Dubois-Violette, P. G. de Gennes, and O. J. Parodi, J. Phys. (Paris) **32**, 305 (1971).

[7] P. A. Penz and G. W. Ford, Phys. Rev. A **6**, 414 (1972).

[8] A. Joets and R. Ribotta, J. Phys. (Paris) **47**, 595 (1986).

[9] W. Zimmermann and L. Kramer, Phys. Rev. Lett. **55**, 402 (1985).

[10] L. Kramer and W. Pesch, in *Pattern Formation in Liquid Crystals*, edited by A. Buka and L. Kramer (Springer, Berlin, 1995).

[11] W. Pesch and L. Kramer, Z. Phys. B **63**, 121 (1986).

[12] E. Bodenschatz, W. Pesch, and L. Kramer, Physica D **32**, 135 (1988); L. Kramer, E. Bodenschatz, and W. Pesch, Comment Phys. Rev. Lett. **64**, 2588 (1990).

[13] W. Decker., Ph.D. thesis, Bayreuth (1995).

[14] E. Plaut, W. Decker, A. G. Rossberg, L. Kramer, W. Pesch, A. Belaidi, and R. Ribotta, Phys. Rev. Lett. **79**, 2367 (1997).

[15] E. Plaut and W. Pesch (unpublished).

[16] H. Richter, A. Buka, and I. Rehberg, Phys. Rev. E **51**, 5886 (1995).

[17] H. Richter, A. Buka, and I. Rehberg, in *Spatio-Temporal Patterns in Nonequilibrium Complex Systems*, edited by P. Cladis and P. Palffy-Muhoray (Addison-Wesley, New York, 1994).

[18] H. Richter, N. Klöpper, A. Hertrich, and A. Buka, Europhys. Lett. **30**, 37 (1995).

[19] Sh. Kai, K. Hayashi, and Y. Hidaka, J. Phys. Chem. **100**, 19 007 (1996); Y. Hidaka, J. Huh, K. Hayashi, M. Tribelsky, and Sh. Kai, J. Phys. Soc. Jpn. **66**, 3329 (1997).

[20] Y. Hidaka, J. Huh, K. Hayashi, Sh. Kai, and M. Tribelsky, Phys. Rev. E **56**, R6256 (1997).

[21] A. Hertrich, W. Decker, W. Pesch, and L. Kramer, J. Phys. II **2**, 1915 (1992); L. Kramer, A. Hertrich, and W. Pesch, in *Pattern Formation in Complex Dissipative Systems*, edited by Sh. Kai (World Scientific, Singapore, 1992).

[22] A. G. Rossberg, A. Hertrich, L. Kramer, and W. Pesch, Phys. Rev. Lett. **76**, 4729 (1996); A. G. Rossberg and L. Kramer, Phys. Scr. **T67**, 121 (1996).

[23] A. Hertrich, Ph.D. thesis, Bayreuth (1995).

[24] A. G. Rossberg, Ph.D. thesis, Bayreuth (1997).
[25] A. G. Rossberg and L. Kramer, Physica D **115**, 19 (1998).
[26] M. Treiber and L. Kramer, Mol. Cryst. Liq. Cryst. Sci. Technol., Sect. A **261**, 951/311 (1995); M. Dennin, M. Treiber, L. Kramer, G. Ahlers, and D. Cannell, Phys. Rev. Lett. **76**, 319 (1995); M. Treiber, N. Eber, A. Buka, and L. Kramer, J. Phys. II **7**, 649 (1997).
[27] M. Treiber and L. Kramer, Phys. Rev. E **58**, 1973 (1998).
[28] S. Rasenat, G. Hartung, B. L. Winkler, and I. Rehberg, Exp. Fluids **7**, 412 (1989).
[29] The calculation was done with programmes by A. Hertrich and W. Pesch.
[30] M. Dennin, D. Cannel, and G. Ahlers, Mol. Cryst. Liq. Cryst. Sci. Technol., Sect. A **261**, 337 (1995).
[31] F. Hörner, Ph.D. thesis, Bayreuth 1997.
[32] M. Scheuring, L. Kramer, and J. Peinke, Phys. Rev. E **58**, 2018 (1998).
[33] R. Faller and L. Kramer, Chaos, Solitons, Fractals (to be published).